International Journal of Engineering & Technology, 7 (3.32) (2018) 137-145

International Journal of Engineering & Technology

Website: www.sciencepubco.com/index.php/IJET

Research paper

Joint Segmentation Methods of Tumor Delineation in PET – CT Images: A Review

Farli Rossi[1]*, Ashrani Aizzuddin Abd Rahni[2]

[1] *Department of Electrical, Electronic and Systems Engineering, Universiti Kebangsaan Malaysia, Bangi, Malaysia*
[2] *Department of Electrical, Electronic and Systems Engineering, Universiti Kebangsaan Malaysia, Bangi, Malaysia*
**Corresponding author E-mail:farli.rossi@gmail.com*

Abstract

Segmentation is one of the crucial steps in applications of medical diagnosis. The accurate image segmentation method plays an important role in proper detection of disease, staging, diagnosis, radiotherapy treatment planning and monitoring. In the advances of image segmentation techniques, joint segmentation of PET-CT images has increasingly received much attention in the field of both clinic and image processing. PET - CT images have become a standard method for tumor delineation and cancer assessment. Due to low spatial resolution in PET and low contrast in CT images, automated segmentation of tumor in PET - CT images is a well-known puzzle task. This paper attempted to describe and review four innovative methods used in the joint segmentation of functional and anatomical PET - CT images for tumor delineation. For the basic knowledge, the state of the art image segmentation methods were briefly reviewed and fundamental of PET and CT images were briefly explained. Further, the specific characteristics and limitations of four joint segmentation methods were critically discussed.

Keywords: *Joint Segmentation; Tumor; PET and CT images; Review.*

1. Introduction

Segmentation is one of the crucial steps in applications of semi-automated or automated tumor diagnosis [70], [71]. The accurate image segmentation method plays an important role in proper disease detection, staging, assessment of disease target volumes, diagnosis, radiotherapy treatment planning, monitoring and follow-ups [34]. Previously, image segmentation approaches were done for a single imaging modality in an example: PET image or CT image alone [4].

Positron Emission Tomography (PET) images have high contrast to non-tumor tissues and therefore make them easily distinguish the malicious area from the normal tissue, however, they are suffered by low spatial resolution and result in poor of target boundary definition of the malicious area [13]. Computed Tomography (CT) images have high spatial resolution that can provide detail information of the human anatomy, however, they are suffered by low contrast from surrounding normal structures and lacking metabolic information which further make them difficult to differentiate between malicious area and normal tissue [34], [75], [7], [47].

Human body, which has complex anatomy cannot be captured accurately in single imaging modality [40]. Combination of two or more imaging modalities can result in higher sensitivity and specificity compared to that component modality alone [40]. In an example, when we use a CT image to segment a lesion which previously has been measured on PET image quantitatively, it can provide more precise texture features in PET-CT images as shown in Fig. 1 [6], [40]. Fig. 1 present the greater contrast of PET image (a), greater spatial resolution of CT image (b), and combination of PET and CT images (c). Due to this reason, integrating between two or more modalities have been widely used now in clinical radiotherapy applications for affective assessment of target volumes in tumor treatment. Therefore, in the advances of image segmentation techniques, joint segmentation of anatomic and functional PET-CT images has increasingly received much attention in the field of both clinic and image processing [47]. Fig. 2 shows an example segmentation that incorporate information from PET and CT images where (a) illustrate the individual segmentation from PET image, (b) illustrate the individual segmentation from CT image, while (c) represent the resulting joint segmentation.

It is obviously shown that the growing interest in integration of PET and CT images has accelerated the methods for segmentation [34]. This paper attempts to describe and reviews four innovative joint segmentation methods of anatomic and functional PET-CT images that are recently used to detect tumor/cancer boundary for achieving accurately region delineations. In supporting the completion of the review, the necessary knowledge about the fundamental principles of PET and CT imaging are given in section 2 while the briefly reviews of state of the art segmentation methods for PET or CT images before developing of joint segmentation methods are represented in section 3. Four innovative joint segmentation methods of anatomical and functional PET-CT images which consist of multivalued level set technique, markov random field (MRF) based technique, random walk co-segmentation technique and combination of low process and active contour technique are further described in section 4 to 8. Finally, the special characteristics and limitations of those joint segmentation methods are discussed in section 9 which followed by conclusion in section 10.

Copyright © 2018 Authors. This is an open access article distributed under the Creative Commons Attribution License, which permits unrestricted use, distribution, and reproduction in any medium, provided the original work is properly cited.

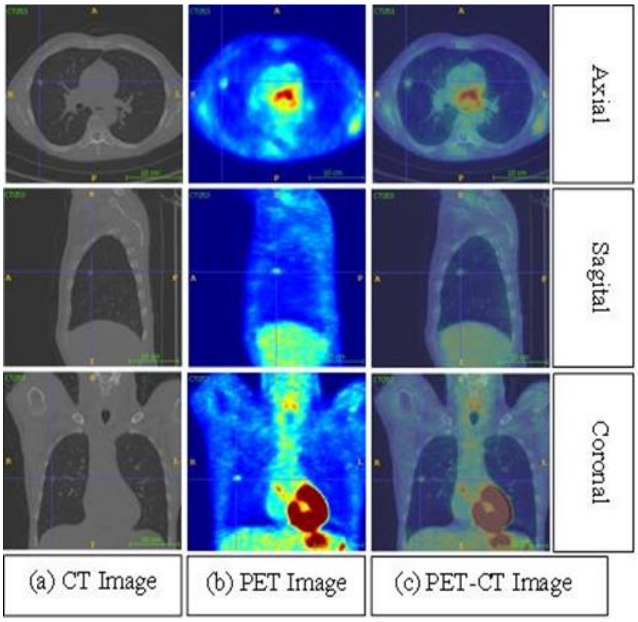

Fig. 1: (a) greater spatial resolution of CT images, (b) greater contrast of PET images, and (c) fusion of PET-CT images.

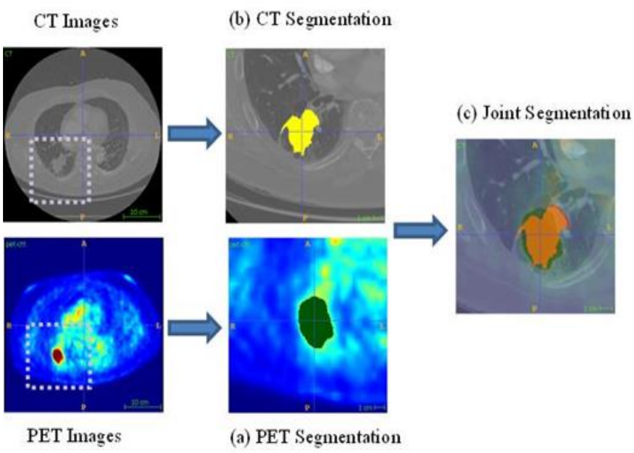

Fig. 2: (a) individual segmentation from PET image, (b) individual segmentation from CT image, and (c) the resulting joint segmentation.

2. Fundamental of PET and CT Images

Computed Tomography (CT) is a structural imaging techniques utilized in clinical practice to observe anatomical abnormalities in human body due to existing of tumor/cancer diseases [34], [7]. CT images give detailed structural information with high spatial resolution about one's anatomy that can be used in purposes of diagnosis and treatment [34], [75]. However, CT images suffer from spatial distortion, lack of physiological/metabolism information and relatively poor soft tissue contrast resolution. It results difficulty in distinguishing the lesion boundary from the normal tissues since tumor intensity will be appeared to be similar to the surrounding soft tissue areas [5]. Therefore, structural imaging of CT is not suitable for pathology detection applications where cellular activity is more significant than anatomical features [54] Previous studies have showed that in CT images, there are a large observed variability of tumor regions due to the similar intensity distribution of tumor with the nearby soft tissues [5], [2].

Regarding to this matter, clinical experts and researchers have developed PET scanners. PET, a Positron Emission Tomography is a non-invasive functional imaging technique which is possible to distribute the biologically targeted radiotracers with high sensitivity and provide detailed physiological information of tumor/cancer diseases [34]. There is several techniques used to measure the cellular metabolism in PET imaging such as SUV (standardized uptake values), TBR (tumor to background ratio), TLE (total lesion evaluation) and etc. [6], [10]. Among them, SUV is the best choice method for quantification of lesions which is relevant measurement of cellular metabolism [61][79][30][68].

PET images have high contrast and therefore makes them easy to differentiate the malignant areas from the normal tissues and reduces the observed variability of tumor sites [31]. PET images are usually used to assess infection of tumor/cancer by identifying the discharged photons from a radiotracer contained to abnormal cells. However, PET images have no good spatial resolution. It cause the target boundary definition from PET imaging is poor and fuzzy and further cannot be used satisfactorily in identifying, diagnosing, characterizing, and staging of the diseases since anatomic boundaries based on structural images are also needed [6], [13]. Therefore, accurate delineation of tumor/cancer volume was going to be difficult by using PET image alone.

Hence, the combination between functional image (PET image) and anatomical image (CT image) is further required frequently in order to identify functional abnormalities and differentiate them from normal extraction of PET radiotracers [34], [60], [51], [50]. Combination of both images leads to a higher sensitivity and specificity than is achievable using either modality alone [34], [48], [31]. In an example, since PET image has no good spatial resolution and therefore cannot accurately indicate the size of lesion or locate any critical anatomical structures that would alter the treatment strategy, however, CT image can properly interpret, localize, visualize and co-evaluate the radiotracer uptake of abnormal regions [6]. In fact, it will be very difficult to differentiate normal tissue from abnormal at CT imaging if the PET image is not provided [6].

The new standard in clinical practice is acquiring PET and CT images instead of a single PET scan to take advantage of the functional and structural information jointly [34]. By combining information of these different modalities which has complementary nature can achieve better radiotherapy treatment planning. Several previous studies have demonstrated that combination of PET and CT images is superior in assessing tumor/cancer disease to reduce variability in target definition [69] and produce a more consistent tumor volumes [81], [35]. Therefore, PET-CT images have increasingly received much attention in the field of both clinic and image processing currently for the effective assessment of target volumes in cancer treatment and has become a standard method of imaging for tumor delineation and cancer assessment [47], [46], [59], [80].

3. Briefly Review of Image Segmentation Methods

In a routine treatment planning procedure, image segmentation methods are required to distinguish tumors to be treated from surrounding normal tissues. Typically, the image segmentation was done manually by the physician to perform the radiotracer uptake regions of target delineation procedure. However, due to time consumption and un-accurate tumor volume delineation from manual segmentation, automated and semi-automated image segmentation techniques are applied [40], [80]. The proper segmentation technique is required to estimate accurately the interest lesion volume of tumor/cancer disease, therefore, many segmentation algorithms has been brought in PET oncology from the Computer Vision field recently [80], [58], [92].

In the clinical practice, the specific characteristics of PET images which are high contrast, fuzzy boundaries of uptake regions and low spatial resolution encouraged thresholding based SUVs techniques to be used in PET image segmentation methods [5], [20], [84]. Thresholding based techniques applied either fixed, adaptive, iterative (ITM) or optimal choice thresholds based on expert interface or phantom simulations [34], [6].

In a fixed based threshold, the SUV's value of 2.5 which is equal to 36 – 40% of the total SUV from predefined region was used in clinical to delineate abnormal area from the background drawn manually [6], [67], [62]. In an adaptive based threshold, realistic phantoms were built by examining class uncertainties in order to provide more optimal thresholding level [66], [56], [21], [17], [73]. For iterative based threshold, iterative thresholding based on scanner hardware properties was applied [25], [83], [45] while for optimal choice based threshold, the local approached was integrating into the threshold selection process [10], [16], [19], [49] to get optimal thresholding levels. It has been shown in various studies [32] that the optimal levels of threshold was the most important in thresholding based methods while the deficiency of optimal threshold levels averts the accuracy of lesion delineations from the background [6]. However, thresholding techniques were generally restricted to delineate a lessons with dimension larger than 4 mL. When the thresholding based techniques were used to segment PET images in lung cancer, it resulted a variation range of 15%−50% in selected threshold value when compared to a CT benchmark [12]. It was also found that thresholding based techniques cannot address uptake heterogeneity, partial volume effect, and tissue inflammation which can strongly influence interpretation of PET images, thus these techniques cannot delineate the tumor volume accurately [12], [74], [55]. More details about segmentation methods based on thresholding approaches for PET images can be found in [34], [6], [91], [74], [14], [68].

Similar to the thresholding approaches, the stochastic and learning-based approaches such as Fuzzy-C-Means (FCM) [90], [11], Fuzzy Locally Adaptive Bayesian (FLAB) [38], clustering [88] and mixture [1] techniques are extensively used in PET image segmentation [6]. It is because the fuzzy nature of lesion boundary such as circular uptake regions is well presented in these approaches [6]. In an example, FLAB which was based on a Bayesian statistical model used a finite number of fuzzy levels to label voxels within a Region of Interest (ROI) [6]. However, although stochastic and learning-based approaches can well segment the circular uptake regions and fuzzy lesion boundary by precisely defining the ROI, the accuracy of delineation algorithms of these approaches are restricted to only large lesions with simple shape while the complex shapes of lesions are not easy to be delineated [6]. Besides**,** a significant problem that arose for these approaches were the lack of a continuous boundary or a spatial neighborhood concept [11], [79]. Specifically in FLAB technique, in order to provide acceptable statistical assessment of voxel labels, the technique requires a significant number of background and foreground voxels within ROI drawn manually [6]. Therefore, the accuracy and capability of these methods in delineating for complex lesion shape are suspected to be more difficult [6].

Apart of the techniques described above, region growing approach [22], gradient based approach [25], [36], level set and active contours approach [44], [52], [48], [26], and graph based approaches [8], [88] are also actively used in clinical applications [6]. In region growing approach [22], [52], the segmented region was assumed to be sufficiently homogeneous, therefore, the results of the segmentation become not accurate and often error for heterogeneous structures. In gradient and contour based approaches, the smooth region with reliable boundary's information was required [6], [36], [48], [26]. Since PET scans produce noisy and not good spatial resolution images, pre-processing techniques are required to be applied in order to reduce noise effects [6]. Based on this, graph based segmentation methods have been proposed in [6], [8], [88] to reduce the difficulty in segmenting complex boundaries on low contrast images and further it has attracted much attention during the last few years in image segmentation due to their good performance [47].

Bagci et al. [8] have demonstrated that a graph based segmentation method using random walk algorithm has effectively segmented lung tumor on PET images [8]. Apart of that, Cherry et al. which have combined the conventional graph cut energy with a novel monotonic downhill function, has showed that the technique has effectively extracted heart and liver [9]. In most of these approaches, foreground seeds, background seeds and ROI are very important to be defined by the user in order to begin and limit the segmentation bounds [6]. Further, active contour and graph based segmentation methods have been superior and promising on PET image segmentation. However, although these advanced image segmentation methods have provided better accuracy compared to thresholding methods, they still have many limitation and the use of these approaches are still avoided from the routine clinical use [6].

Overall, all approaches of image segmentation methods mentioned earlier are developed only on functional PET images without concerning the integration of anatomical information (in example CT image) into the segmentation process [6]. Recently, it is highly required to have both functional and structural information in clinical uses to provide more accurate of disease identifications and delineations for potentially resulting in an earlier diagnosis and more effective treatment plan [6]. Inline to the developments of multi-modal scanners (in example PET-CT), there are recent attempts in the literature to take the advantages of integrating anatomical and functional information for separating the abnormal regions (lesions) from normal structures [71], [34], [6], [7], [40], [89], [47].

4. Join Segmentation Methods of Functional and Anatomical PET - CT Imaging a Step Before the Final Submission

Due to the information given in PET and CT images are different but complementary, the combination of single modality of PET and CT images provides great potentials to the fields of segmentation [40]. Based on the section 2 and section 3 above, the number of developers have recommended that the integration of information from both PET and CT images would provide more accurate segmentation results compared to use of single modality alone [74]. Because of this, there are many joint segmentation techniques of functional and anatomical PET-CT imaging that have been proposed recently as motivated in achieving more accurate tumor volume detection/delineation from segmentation results and improve the robustness of the segmentation process. In an examples, a handful of algorithms exist named as multivalued level set (MVLS) [26], an algorithm of Markov Random Field formulated on a graph [40], the variational Bayes inference technique [85], voxel-by-voxel basis technique [86], random walk co-segmentation [6],[7], PET and CT combination of Textural Features technique [74], [89], Combination of Random Walk and Graph Cut techniques [47] and combination of low level process and active contour [70], [71].

In this paper, we attempt to expose and review four famous techniques in joint segmentation methods of functional and anatomical PET and CT images among all available techniques due to their specific characteristics which consist of Multivalued Level Set technique, Markov Random Field (MRF) Based technique, random walk co-segmentation technique and combination between low level process and active contour technique.

5. Multivalued Level Set Technique

5.1. Background

El Naqa et al., [26] developed a joint segmentation technique of PET and CT images based on the level set approach by applying active contour techniques. The level set is a method which defines sets of contour values and positions that evolve over time [28]. Level sets were initially developed in theory of curve evolution to resolve the restrictions faced in parametric deformable models [28]. These characteristics have allowed the level set techniques to represent the state-of-the-art in shape recovery applications [3], [64], [82].

Mathematically, if the deformable contour/surface at a time $t \geq 0$ is represented by $C(c , t) = \{x(c , t) , y(c , t) , z(c , t)\}$, $s \in[0,1]$ then according to the curve evolution theory, its movement could be represented by the following partial differential equation as shown in (1) [52]:

$$\frac{\partial C(c,t)}{\partial t} = \vec{V}(K) \tag{1}$$

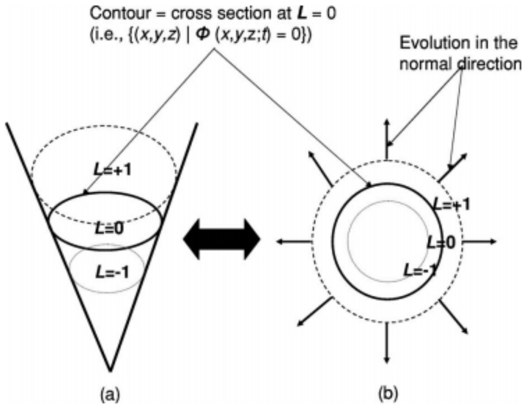

Fig. 3: Deformable image segmentation by using the level set technique

Fig. 3 illustrates the principle of deformable image segmentation by using the level set technique: a) representation of the level set surface at time t of the evolving function and (b) a projected view showing the evolution direction.

5.2. Multimodality Image Segmentation by the Level Set Method (MVLS)

The definition issues of spatial neighborhood faced in clustering methods was inherently corrected in active contour methods [26]. However, in active contour methods, multi-modality imaging generalization was based on redefining the concept of boundary as a logical combination of multiple images [26]. For this reason, MVLS approach was adapted which was originally developed to handle multichannel color images [77], [18].

In the previous work, Naqa et al., [27] used the level set method for auto-segmentation of single image. They noticed that more robust results were achieved when direct gradient based methods for estimating image boundaries were replaced or combined with methods that do not require noisy explicit image gradients. For this, Naqa et al., [27] applied edge-modeling (region-based) techniques to improve robustness to noise. For generalization of the level set, Naqa et al., used (2) in segmentation of N multi-modality images [23].

$$\begin{aligned} &\mathrm{Inf_l}\ (\mathrm{L}, \mathrm{l}^+, \mathrm{l}^-) \alpha\eta \ \text{length (L)} \\ &+ \frac{1}{N} \sum\nolimits_t \chi_i^+ \int_\Omega \left| I_i - l_i^+ \right|^2 H(\phi) dx + \chi_i^- \\ &x \int_\Omega \left| I_i - l_i^- \right|^2 (1 - H(\phi) dx) \end{aligned} \tag{2}$$

where η is a weighting factor for the contour length given by the surface integral in 3D (or the line integral in 2D). H is the Heaviside function which is following:

$$H(x) = \begin{cases} 1, & x \geq 0 \\ 0, & otherwise \end{cases} \tag{3}$$

(in the implementation, this is approximated by a smooth inverse tangent function), $l_i^+ (l_i^-)$ corresponds to the pixel intensity means inside (outside) of the contour, and χ_i^+ (χ_i^-) are user-defined parameter pairs providing relative "importance weights" based on the user's experiences, assigned for each of the imaging modalities in contrast with the other modalities [26]. The last term corresponds to the spring force and is thought to provide further balance by introducing more inside: outside contour contrast by adjusting Ω_i. $Inf_l$is the infimum of the set of possible contours (L) solutions satisfying the functional. Infimum is the greatest lower bound of a set. This is more accurate than using the minimum, which does not necessarily exist in this case.

Potentially, numerous logical integrations of images could capture the basic biophysical structure [23]. Naqa et al., have applied a soft-AND model where is the logical combination of the images was determined by the assigned relative weights (χ_i) as shown in (3) [23]. The weights were intended to reflect the ability in assigning images with lower contrast (i.e., CT) to be a similar computational importance as images with greater contrast (MRI, PET) based on the user's experiences. Nevertheless, other factors may also be important. Obviously, the selection of weights will presumably be based on experience and training gained using the technique and better understanding of the conceptual mapping in (4).

$$Biophysical\ structure = f(CT, PET, \dots;\ \chi\,) \tag{4}$$

The MVLS algorithm started with an initial contour in the multi-image domain. The curve was changes under the effect of the internal forces (contour curvature and string force) and external forces (image boundaries) until they reached equilibrium [26]. Default weighting (η) was applied to the contour curvature to maintain acceptable elasticity (smoothness) of the contour and the spring force was fixed for the different imaging modalities. However, it is noticed that the solution to the curve evolution (in (2)) does not necessarily guarantee that the evolving function $\phi(.)$ will remain a valid distance function, which could potentially cause serious numerical problems such as unbounded gradients. Hence, they followed the approach of Aujol et al. in rebuilding the distance function such that the zero level was maintained at the current solution for the evolving function $\phi(C, t_c)$ as shown in (5).

$$\frac{\partial\varphi}{\partial t} + sign(\phi(C, t_c)(|\nabla\varphi| - 1)) = 0 \tag{5}$$

where the PDE in (5) is initialized with the current level set solution at time t_c [i.e., $\varphi(C, 0) = \phi(C, t_c)$] and the solution φ (as t tends to infinity) would yield the evolving function with corrected distance function that will be used to reinitialize (2). Upwinding finite difference schemes were used to approximate $|\nabla\varphi|$, where a one-sided (back-ward or forward) finite difference is used in accordance with the sign of $\phi(C, t_c)$. This reinitialization process is repeated every 10 or 20 iterations.

6. Markov Random Field (MRF) based method

6.1. Background

Han et al., [40] have developed a formulation as a double labeling of MRF on a graph for co-segmentation of PET – CT images purposes [39]. The formula was named as MFR segmentation energy which was applied to minimize the MRF total energy in PET and CT imaging and solving the different results of segmentation between PET and CT images [39]. Here, a divergent random variable f_x is announced for each voxel x as a input in PET and CT images [39]. By denoting f_{PET} (which is respective to f_{CT}), the variable sets is related to the voxels in the input PET (which is respective to CT) image [39].

In the phase of pre-processing, Han et al. applied algorithm of image registration. It is applied in order to register PET image to the CT image and make sure that there is same size between both CT and PET images by assuming one to one correspondence between f_{PET} and f_{CT} [39]. They denoted the voxels x' in the CT image corresponding the voxels x in the PET image. Each label f in PET image (f_{PET}) and CT image (f_{CT}) is taking a label value from the label set $\mathcal{L}$ = {0, 1} representing that the voxels are in background with f = 0 and in the foreground with f = 1 [39]. Then, every possible task of the random variables in f_{PET} (which is respective tof_{CT}) delineate the tumor region in the PET (which is respective to CT) image [39]. Han et al., applied the method of Boykov and Funka-Lea's graph cuts to optimally calculate the tumor segmentation in PT image or CT image which is done separately [39], [15].

Further, Han et al., [40] introduced a third set of co-segmentation (for dual variables f_{PET-CT}) as a pair voxels x and x' in the PET and CT images to take advantages of the both modalities for segmentation [40], [39]. f_{PET-CT} integrated the energy consequence of the disagreement of the PET and CT segmentation distinction. However, there is no consequence that will be enforced if the pair labels of voxels (x, x′), f_x and $f_{x'}$ are the same [39]. In the final results of the co-segmentation, PET and CT might be weighted differently and therefore the different consequences of the disagreement might be enforced [39]. Hence, the big issue in this approach is to minimize the energy function as following [39]:

$$\varepsilon_{PET-CT} = E_{PET}(f_{PET}) + E_{CT}(f_{CT}) + E_{PET-CT}(f_{PET-CT}) \quad (6)$$

$\boldsymbol{E_{PET}}$ $(\boldsymbol{f_{PET}}$) and $\boldsymbol{E_{PET}}$ $(\boldsymbol{f_{CT}}$) are energy functions of the MRF for the PET and CT, respectively while $\boldsymbol{E_{PET-CT}}$ $(\boldsymbol{f_{PET-CT}}$) is co-segmentation energy that be used to integrate the consequences of disagreement of the segmentation distinctions between the PET (with high contrast) and CT (with high spatial resolution) [39].

6.2. Energy Segmentation of MRF for the PET

By denoting ξ_{PET} as surrounding system which is used in PET image input ζ_{PET}, the energy function of MRF ($\boldsymbol{E_{PET}}$ $(\boldsymbol{f_{PET}}$)) is defined as following [39]:

$$\mathrm{E_{PET}}(f_{PET}) = \sum_{r \in \zeta_{PET}} d_r(f_r) + \sum_{(r,s) \in \xi_{PET}} w_{r,s}(f_r, f_s) \quad (7)$$

$\boldsymbol{d_r(f_r)}$ and $\boldsymbol{w(f_r, f_s)}$ are data and smoothness term [39], [78]. Smoothness calculates the cost of set different labels to neighbor voxels r and s in ζ_{PET} as presented in [39].

$$w_{r,s}(f_r, f_s) = \begin{cases} \varepsilon(r,s) & if \ f_r \neq f_s \\ 0 & if \ f_r = f \end{cases} \quad (8)$$

6.3. Energy Segmentation of MRF for the CT

By denoting ξ_{CT} as surrounding system which is used in CT image input ζ_{CT}, the energy function of MRF $\boldsymbol{E_{CT}}$ $(\boldsymbol{f_{CT}}$) is defined as following .

$$\mathrm{E_{CT}}(f_{CT}) = \sum_{r \in \zeta_{CT}} d_{r'}(f_{r'}) + \sum_{(r',s') \in \xi_{CT}} w_{r',s'}(f_{r'}, f_{s'}) \quad (9)$$

6.4. Co-Segmentation Energy of MRF

$\boldsymbol{E_{PET-CT}}$ $(\boldsymbol{f_{PET-CT}}$) integrates the consequence of disagreement of the segmentation distinction between the PET ζ_{PET} and the CT ζ_{CT} [39]. The variable $f_{(r,r')} \in f_{PET-CT}$ is related to the pair voxels (r, r′) in ζ_{CT} and ζ_{PET} which takes a value from the label set $\mathcal{L}$ = {0, 1} [39]. If $f_{(r,r')} = 1$, the voxels r and r' are categorized as foreground (tumor) while for others, the voxels r and r' are categorized as background [39]. Here, Han et al., used the function $\gamma_{r,r'}(f_r, f_{(r,r')}, f_{r'})$ ((10)) for penalizing the differences of f_r and $f_{r'}$ and attempt to resolve it based on the outstanding features of the PET and CT [39].

$$\gamma_{r,r'}(f_r, f_{(r,r')}, f_{r'}) = \begin{cases} 0, \text{ if } \ f_r = f_{(r,r')} = f_{r'} \\ \varphi_1(r,r'), \text{ if } \ f_r \neq f_{r'} f_{(r,r')} = f_{r'} \\ \varphi_2(r,r'), \text{ if } \ f_r \neq f_{r'} f_{(r,r')} = f_r \end{cases} \quad (10)$$

φ_1 (r, r′) and φ_2 (r, r′) are the respectively values used in penalizing the distinctions of the segmentation between r and r' while the co-segmentation energy is defined as following [39]:

$$\mathrm{E}_{PET-CT}(f_{PET-CT}) = \gamma_{r,r'}(f_r, f_{(r,r')}, f_{r'}) \quad (11)$$

7. Random Walk Co-Segmentation Technique

7.1. Background

Bagci et al., [7] have proposed a co-segmentation technique in integrating the advantages of both PET and CT modalities by developing an algorithm based on random walk methods. This technique is applied to delineate the accurate tumor volume with correct structural boundaries [75]. Further, the automatic of seed localization of background or foreground is also proposed to provide fully automatic for the whole system.

7.2. Co-Segmentation Based on Random Walk

A graph GR is denoted as a pair GR = (VE, ED) while v ϵ VE represents the vertices/nodes and e ∈ ED ⊆ VxV represents the edges. If a node v (consist of v_u and v_v) is linked to an edges e_{uv} in graph GR, so v_u could be declared as a neighbor to the v_v and each edge is weighted by w_{uv}. Here, a graph GR is assumed to be connected and un-directed, so that w_{uv} shoud be equal to w_{vu}. Bagci et al., formulate separately the weighting functions for the PET and CT modalities based on recommendation by Grady [37] as following

$$\begin{aligned} w_{uv}^P &= \exp(-\beta^P (In_u^P - In_v^P)^2) \\ w_{vu}^C &= \exp(-\beta^C (In_u^C - In_v^C)^2) \end{aligned} \quad (12)$$

In_u denotes the intensity at u-direction and β denotes a weighting factor while P and C indicate the PET and CT imaging modality, respectively. Conventionally, the probabilities of random walk are required to be similar solutions with the problem of combinatorial Dirichlet as presented in (13) [45]:

$$D[x] = \frac{1}{2} x^T L x \quad (13)$$

x indicates the probability of each node [42] while L indicates the combinatorial Laplacian matrix. For each of the functional and anatomical imaging modalities, this matrix can be constructed as in (14):

$$L_{uv}^Z = \begin{cases} d_u^Z & if \ u = v \\ -w_{uv}^Z & if \ v_u^Z \text{ and } v_v^Z \text{ are nearby nodes} \\ 0 & otherwise \end{cases} \quad (14)$$

Z is one modality whether it is PET or CT alone, so Z ∈ PET or CT. $d_u = \sum_{e_{uv}\in E} w(e_{uv})$, is the vertex degree [75]. v^P is the node connecting to the graph constructed on PET imaging and $v^C$is the node connecting to the graph constructed on CT imaging.

In segmentation of combined PET-CT imaging modalities based on the graph, a graph need to represent the complete information from both PET and CT imaging. Based on graph theory, two graphs (graphs for PET and CT) can be integrated if an edge exists in both graphs [45]. By denoting two graphs $GR^P = VE^P, ED^P$ (for PET) and $GR^C = VE^C, ED^C$ (for CT), the fuse graph from the both graphs can be defined as $GR^{FS} = VE^{FS}, ED^{FS}$. The following formulation is subjected to the fuse graph,

$$v^{FS} = \{(v_u^c, v_u^p) : v_u^c \in v^p \in V^p\}$$
$$E^{FS} = \{(v_u^c, v_u^p), (v_v^c, v_v^p)\} : (v_u^c, v_v^c) \in E^c \Lambda (v_u^p, v_v^p) \in E^p\} \quad (15)$$

Instead of using a separate implementation of GR^C and GR^P, Bagci et al., applied the fuse graph GR^{FS} to segment objects simultaneously. The combinatorial Laplacian matrix (L^{FS}) for the fuse graph GR^{FS}can be defined as following:

$$L^{FS} = (L^C)^\alpha \otimes (L^p)^\theta \quad (16)$$

L^{FS} is assumed to be constant for $\alpha \geq 0$ and $\theta \leq 1$ while ⊗ indicates the direct product. By denoting x^C and x^P as distribution of initial probability over the graph nodes of GR^C and GR^P, the distribution of initial probability for fuse graph x^{FS} is following (17). ζ and η are applied to optimize the distributions of initial probability which has limitation by ζ ≥ and η ≤ 1.

$$x^{FS} = (x^C)^\zeta \otimes (x^p)^\eta \quad (17)$$

The performance of a random walk on the fuse graph GR^{FS} is assumed to be equal to the performance of simultaneous random walk on the graphs GR^C and GR^P [45]. Furthermore, the combinatorial formulation of Dirichlet integral can be updated as following:

$$D[x^{FS}] = \frac{1}{2}(x^{FS})^T L^{FS} x^{FS} = \frac{1}{2} \sum_{e_{uv}\in E^{FS}} w_{uv}^{FS} (x_u^{FS} - x_v^{FS})^2 \quad (18)$$

By considering separately the prior probabilities and Laplacian matrices of unlabeled and labeled nodes, Bagci et al., decompose (18) as following in (19).

$$D[x_r^{FS}] = \frac{1}{2}(x^{FS})_l^T (x^{FS})_r^T = \begin{bmatrix} L_l^{\backslash FS} & B \\ B^T & L_r^{FS} \end{bmatrix} \begin{bmatrix} x_l^{FS} \\ x_r^{FS} \end{bmatrix} \quad (19)$$

In the matrix decomposition ($\boldsymbol{L^{FS}}$), sub-matrix is denoted by B. The results show that the combinatorial Laplacian matrix $\boldsymbol{L^{FS}}$ is semi-definite with positive amount while the critical points of $\boldsymbol{D}[\boldsymbol{x^{FS}}]$ are the minimal.

8. Combination of Low Level Processing and Active Contour Technique

Rossi et al, [70], [71] have proposed a semi-automated joint segmentation technique of thoracic PET and CT imaging. This technique combined the models of low level process with active contour in order to extract the lung lesions from thoracic PET-CT imaging modalities. Here, deformation in active contour model is influenced by internal force-like equations [39], [76], [87] while the image intensity of the contours have a incisive variations corresponding to minimize the energy for matching the deformed and reference contours [91], [3], [64], [87].

In this approach, the purposed segmentation consist of two-fold; firstly as a guide for the image registration process and secondly to provide a brief anatomical segmentation for lesion segmentation. For the first fold, there are three steps involved in the overall image segmentation which are consist of a) automated multiple thresholding, b) respiratory system extraction and c) pulmonary three extraction. In the automated multiple thresholding step, Otsu's method [65] and connect component analyses (CCA) [43] were used. In the respiratory system extraction step, an initial lung region was obtained while the pulmonary tree such as blood vessels was obtained from the pulmonary tree extraction. The detail information about this technique can be found at Rossi et al., [70], [71].

Second fold is lesion segmentation. For lung segmentation, firstly SUV image is obtained from the initial PET activity image using the standard formula:

SUV = C/(D/W)

C indicates the concentration from the PET activity image while the injected dose and the body weight are denoted by D and W, respectively. The activity image is first decay corrected before calculation of the SUV.

The SUV image is then threshold using Otsu's method over the whole image or within a specified region of interest around the lesion. Using Connect Component Analyses (CCA), the lesion is manually selected. In case from thresholding the lesion is connected to other components, the boundary can be refined using the Chan-Vese active contour (CV-AC) [18] method which is initialized from the center of lesion found the distance transform. As the lesion is segmented based on the SUV image, it is then used as an initial contour for the AC-AC method for segmentation based on the thoracic CT image. This sequential segmentation approach is used in consideration of the scans potentially being largely separated in time. In cases where the lesion is on the lung boundary, a balloon active contour (B-AC) is first used [53], guide by the initial overall segmentation. After which only is the CV-AC method is then used. This is to prevent the contour propagating beyond the lung boundary.

9. Discussion

In this section, we would like to discuss about the specific characteristic and available limitation of four innovative join segmentation methods of PET-CT images. First method is named multi-valued level set which was developed by El Naqa et al., [26]. This technique was proposed based on deformable models of active contour and also method of generalized single-modality variation. The delineation of tumor volumes by using this technique result an increasing robustness to image noise and a decreasing gaps to the boundaries. This method also has inherent sub-pixel accuracy due to their spatially continuous representation. Furthermore, since multi-modality structures which refer to "biophysical structure" were used, the algorithm applied in this approach is well worked in presence of heterogeneous uptakes with small miss-registration error. However, this method is suited well to be applied in head and neck cancers, while for lung cancer cases (which have heterogeneity in lung region), this technique needs highest image resolution in example 4D image.

The second method of joint segmentation reviewed in this paper was proposed by Han et al., [40]. Han et al., have developed an optimal graph based co-segmentation method by establishing a mechanism of arbitration graph, encoding the characterized information of PET and CT images and combining the context information between both images. This technique was based on algorithms developed to optimize and solve the problem of MRF (Markov Random Field). An arbitration term in the energy function was used in this technique to produce a reliable contour for both PET and CT which further result a single reliable tumor volume from PET and CT images. However, this technique may not provide the accurate results in tumor boundary delineation since it assumed one-to-one correspondence between PET and CT delineations and compromised the identical tumor volume calculated in both PET and CT images. It is because the uptake region calculated in PET images cannot be credited to be always same compared to outlines of lesions calculated in CT images due to the functional characteristics of the tumor. Besides, this technique only can be applied to head and neck tumor/cancer with non-small size because the performance to delineate the small uptake regions of tumor was not evaluated.

The third method of joint segmentation discussed in this paper is random-walk co-segmentation proposed by Bagci et al., [7]. Bagci et al., [7] have developed a co-segmentation technique of combined single modality of PET and CT imaging based on random walk segmentation method by constructing the hyper graph. Here, the technique treated the image as a graph and a weight graph was constructed. Although the mathematical concept used in this technique was different with Han et al., [40], but, the natural adaptation to the proposed segmentation algorithm of this approach is similar. The best advantage of this approach is when the one-to-one correspondence between functional and anatomical structures is not satisfied, this approach can adapt the algorithm to solve that problems. By using a co-segmentation algorithm, it has increased sturdiness into the process of lesion delineation due to unification of the information from both PET and CT imaging. Besides, co-segmentation provides wider spatial and temporal coverage of the tissues with less uncertainty and therefore offers more reliability in results. All these advantages are due to the reality that co-segmentation algorithms can be applied to imitate the appearance of human visual image recognition which depends on the number of informative features such as corners, texture, edges, and lines which are available in the images.

Three innovative joint segmentation techniques mentioned earlier attempt to provide systematically and accurately non-small tumor delineation especially on neck and brain PET and CT images. For delineating lung cancer, Rossi and Abd. Rahni [70] and Rossi et al., [71] have proposed a semi-automated joint segmentation method of thoracic PET and CT images by combining low level process and active contour. This technique based on deformable models which geometric representations were defined explicitly in the imaging domain. In this approach, the impact of internal force-like equations will deforms the models while the contours are characterized by sharp variations in the image intensities to match deformed and reference contours by method of energy minimization. However, this technique was only examined using few data sets while more data sets should be tested to present its performance in accurate segmentation result. Besides, since this technique is semi-automated, the lung boundary should be well defined, otherwise there might be difficulty to delineate lesion boundary properly. The improvement of current technique to be automated joint segmentation method will guarantee more accuracy in the segmentation result.

Overall, all of the joint segmentation methods mentioned in this discussion attempt to combine the complementary information from both PET and CT images in order to define accurately the tumor volumes from the human body normal structures. The first three methods are the famous methods in tumor delineation which keep using and improving by other researches recently. However, these three methods only give best accuracy in tumor volume delineation for neck and head tumors with non-small sizes while there is no evaluation done for the first two methods in volume delineation of lung tumors (small or non-small sizes) since delineation of the lung tumor is more difficult. Besides, there was an evaluation done for the third method in delineation of non-small lung tumor and the results showed that the third method given acceptable accuracy but it is not the best accuracy yet. As we know that lung tumor is not homogeneities in the lung region and has similar densities in pulmonary structures such as bronchioles, bronchi, arteries and veins; therefore the technique used in delineation of lung tumor/cancer should be more specific and it is still keep developing recently by researchers and clinical. One example of the technique used in delineation of lung tumor is that has been proposed by Rossi and Abd. Rahni. However, the best accuracy for lung tumor volume delineation is still a task especially for small tumor sizes.

10. Conclusion

An accurate image segmentation method is required for diagnostic assessment. Since interest in integration of PET and CT images has accelerated, it is appear that joint segmentation techniques of PET-CT images has attracted increasing attentions in clinical application. It is due to the superior of its results segmentation in tumor volume delineation obtained by combining two complementary modalities. However, although many joint-segmentation have been developed and proposed recently, the best method of automatic joint segmentation on PET-CT images in delineation of tumor volume is still a puzzling. Especially for lung tumor/cancer where the tumor is highly integrated into the mediastinum, shows heterogeneous uptake, or is surrounded by collapsed lung or in lamed tissue and when the size tumor/cancer is small. Therefore, research in image segmentation method areas will keep continuing due to accuracy, precision and efficiency in tumor/cancer volume delineation.

Acknowledgement

The authors sincerely thank to Ministry of Education Malaysia and Universiti Kebangsaan Malaysia (grant no. GGPM-2013-066) for the support in completing the research.

References

[1] Aristophanous M, Penney BC, (2007), Martel MK, Pelizzari CA, "A gaussian mixture model for definition of lung tumor volumes in positron emission tomography", *Med Phys*, Vol.34, pp. 4223–4235.

[2] Ashamalla H, Rafla S, Parikh K, Mokhtar B, Goswami G, Kambam S, Abdel HD, Ross AP, Evola A, (2005), "The contribution of integrated PET/CT to the evolving definition of treatment volumes in radiation treatment planning in lung cancer", *International Journal of Radiation, Oncology, Biology and Physics*, Vol.63(4), pp.1016–1023.

[3] Aubert G, (2006), *Mathematical Problems in Image Processing: Partial Differential Equations and the Calculus of Variations*, 2nd ed., Springer, New York,

[4] Aujol J and Aubert G, (2002), "Signed distance functions and viscosity solutions of discontinuous Hamilton–Jacobi equations", Technical Report No.4507, (unpublished)

[5] Baardwijk AV, Dooms C, Suylen RJV, et al, (2007), "The maximum uptake of (18)F-deoxyglucose on positron emission tomography scan correlates with survival, hypoxia inducible factor-1alpha and GLUT-1 in non-small cell lung cancer", *Eur J Cancer*, Vol.43, pp. 1392–1398.

[6] Bagci U, Udupa JK, Mendhiratta N, Foster B, Xu Z, Yao J, Chen X and Mollura DJ, (2013), "Joint segmentation of anatomical and functional images: Applications in quantification of lesions from PET, PET-CT,

MRI-PET, and MRI-PET-CT images", *Medical Image Analysis*, Vol.17, pp.929–945.

[7] Bagci U, Udupa JK, Yao J, Mollura DJ, (2012), "Co-segmentation of functional and anatomical images", *Proceeding of Medical Image Computing and Computer-Assisted Intervention–MICCAI, Springer*, pp: 459–467.

[8] Bagci U, Yao J, Caban J, Turkbey E, Aras O, Mollura D, (2011), "A graph-theoretic approach for segmentation of pet images", *Engineering in Medicine and Biology Society, EMBS, Annual International Conference of the IEEE*, pp. 8479–8482.

[9] Ballangan C, Wang X, Fulham M, Eberl S, Feng D, (2013), "Lung tumor segmentation in PET images using graph cuts," *Computer Methods and Programs in Biomedicine*, Vol. 109, pp. 260–268.

[10] Basu S, Kwee T, Surti S, Akin E, Yoo D, Alavi A, (2011), "Fundamentals of pet and pet/ct imaging", *Annals of the New York Academy of Sciences*, Vol.1228, pp.1–18.

[11] Belhassen S and Zaidi H, (2010), "A novel fuzzy c-means algorithm for unsupervised heterogeneous tumor quantification in PET", *Medical Physics*, Vol. 37(3), pp. 1309–1324.

[12] Biehl K, Kong F, Dehdashti F, Jin J, Mutic S, ElNaqa I, Siegel B, Bradley J, (2006), "18f-FDG PET definition of gross tumor volume for radiotherapy of non-small cell lung cancer: is a single standardized uptake value threshold approach appropriate?", *J Nucl Med*, Vol. 47 (11), pp. 1808–1812.

[13] Boellaard R. Krak N, Hoekstra O, Lammertsma A, (2004), "Effects of noise, image resolution, and ROI definition on the accuracy of standard uptake values: a simulation study", *Journal of Nuclear Medicine*, Vol.45, pp.1519–1527.

[14] Boudraa A, Zaidi H, (2006), *Image segmentation techniques in nuclear medicine imaging, in: Zaidi (Ed), Quantitative analysis ofnuclear medicine imaging*, Springer, New York, pp:308–357.

[15] Boykov Y, Funka-Lea G, (2006), "Graph cuts and efficient and image segmentation", *International Journal of Computer Vision*, Vol.70, pp.109–131.

[16] Bradley JD, Perez CA, Dehdashti F, and Siegel BA, (2004), "Implementing biologic target volumes in radiation treatment planning for non-small cell lung cancer", *J Nucl Med*, Vol.45, pp.96S–101S.

[17] Brambilla M, Matheoud R, Secco C, Loi G, Krengli M, Inglese E, (2008), "Threshold segmentation for PET target volume delineation in radiation treatment planning: the role of target-to-background ratio and target size", *Med Phys*, Vol. 35 (4), pp.1207–1213.

[18] Chan TF, Sandberg BY, and Vese LA, (2000), "Active contours without edges for vector-valued images", *J. Vis. Commun. Image Represent*, Vol. 11, p.130–141.

[19] Ciernik I, Huser M, Burger C, Davis J, Szekely G, (2005), "Automated functional image-guided radiation treatment planning for rectal cancer", *International Journal of Radiation Oncology, Biology, Physics*, Vol 62, pp.893–900.

[20] Daisne J, Sibomana M, Bol A, Doumont T, Lonneux M, Grégoire V, (2003), "Tri-dimensional automatic segmentation of PET volumes based on measured source-to-background ratios: influence of reconstruction algorithms", *Radiother Oncol*, Vol.69(3), pp.247–250.

[21] Davis J, Reiner B, Huser M, Burger C, Szekely G, Ciernik I, (2006), "Assessment of 18f PET signals for automatic target volume definition in radiotherapy treatment planning", *Radiother Oncol*, Vol. 80, p. 43–50.

[22] Day E, Betler J, Parda D, Reitz B, Kirichenko A, Mohammadi S, Miften M, (2009), "A region growing method for tumor volume segmentation on pet images for rectal and anal cancer patients", *Medical physics*, Vol. 36, p.4349

[23] Deasy JO, Yang D, El Naqa I, (2007), "Automated estimation of the biophysical target for radiotherapy treatment planning using multimodality image analysis", *Proceeding of 2007 IEEE International Conference on Image Processing*, pp:V533-V536

[24] Drever L, Robinson D, McEwan A, Roa W, (2006), "A local contrast based approach to threshold segmentation for PET target volume delineation" , *Med Phys*, Vol.33(6), pp.1583–1594.

[25] Drever L, Roa W, McEwan A, Robinson D, (2007), "Iterative threshold segmentation for PET target volume delineation", *Med Phys*, Vol. 34 (4), pp. 1253–1265.

[26] El Naqa I, Yang D, Apte A, Khullar D, Mutic S, Zheng J, Bradley J, Grigsby P, Deasy J, (2007), "Concurrent multimodality image segmentation by active contours for radiotherapy treatment planning", *Medical Physics*, Vol. 34, pp. 4738

[27] El Naqa I, Bradley J, Deasy J, Biehl K, Laforest R, and Low D, (2004), "Improved analysis of PET images for radiation therapy", *Proceeding of 14th (ICCR) International Conference on the Use of Computers in Radiation Therapy, Seoul, Korea*, Vol. 1, pp: 361–363.

[28] El Naqa I, (2010), "Variational methods for image guide adaptive radiotheraphy", *Proceeding of IEEE Southwest Symposium on Image Analyses & Interpretation (SSIAI)*, pp: 13-16

[29] Erdi YE, Mawlawi O, Larson SM, Imbriaco M, Yeung H, Finn R, and Humm JL, (1997), "Segmentation of lung lesion volume by adaptive positron emission tomography image thresholding", *Cancer*, Vol.80, pp.2505–2509

[30] Erdi YE, Rosenzweig K, Erdi AK, Macapinlac HA, Hu Y, Braban LE, Humm JL, Squire OD, Chui C, Larson SM, Yorke ED, (2002), "Radiotherapy treatment planning for patients with non-small cell lung cancer using positron emission tomography (PET)", *Radiotherapy and Oncology*, Vol.62(1), pp.51–60.

[31] Evanko D, (2008), "Two pictures are better than one", *Nat Methods*, Vol.5(5), pp.377.

[32] Fahey F, Kinahan P, Doot R, Kocak M, Thurston H, Poussaint T, (2010), "Variability in pet quantitation within a multicenter consortium", *Medical physics*, Vol. 37, pp.3660.

[33] Ford E, Kinahan P, Hanlon L, Alessio A, Rajendran J, Schwartz D, Phillips M, (2006), "Tumor delineation using PET in head and neck cancers: threshold contouring and lesion volumes", *Med Phys*, Vol.33, pp.4280–4288.

[34] Foster B, Bagci U, Mansoor A, Xu Z, Mollura DJ, (2014), "A review on segmentation of positron emission tomography images", *Computers in Biology and Medicine*, Vol.50, pp 76–96.

[35] Fox J, Rengan R, O'Meara W, Yorke E, Erdi Y, Nehmeh S, Leibel S, Rosenzweig K, (2005), "Does registration of PET and planning CT images decrease interobserver and intraobserver variation in delineating tumor volumes for non-small-cell lung cancer?", *Int J Radiat Oncol Biol Phys*, Vol.62(1), pp.70–75

[36] Geets X, Lee J, Bol A, Lonneux M, Grégoire V, (2007), "A gradient-based method for segmenting fdg-pet images: methodology and validation", *European journal of nuclear medicine and molecular imaging*, Vol. 34, p.1427–1438.

[37] 87Grady L, (2006), "Random Walks for Image Segmentation", *IEEE Transactions on Pattern Analysis and machine Intelligence*, Vol.28, No.11, pp.1768–1783.

[38] Hatt M, Cheze le Rest C, Turzo A, Roux C, Visvikis D, (2009), "A fuzzy locally adaptive bayesian segmentation approach for volume determination in pet", *Medical Imaging, IEEE Transactions*, Vol. 28, p.881–893.

[39] Han D, (2011), *Globally optimal tumor segmentation in PET-CT images: A graph based co-segmentation method*, Lecture notes in computer science

[40] Han D, Bayouth J, Song Q, Taurani A, Sonka M, Buatti J, Wu X, (2011), "Globally optimal tumor segmentation in PET-CT images: A graph-based co-segmentation method", *Information Processing in Medical Imaging*, pp.245–256.

[41] Harary F, (1994), *Graph Theory*, ABP

[42] Hong R, Halama J, Bova D, Sethi A, Emami B, (2007), "Correlation of PET standard uptake value and ct window-level thresholds for target delineation in CT-based radiation treatment planning", *Int J Radiat Oncol Biol Phys*, Vol.67(3), pp.720–726.

[43] Horn BKP, (1986), *Robot Vision*, MIT Press, pp:69-71.

[44] Hsu C, Liu C, Chen C, (2008), "Automatic segmentation of liver PET images", *Computerized Medical Imaging and Graphics*", Vol. 32(7), pp.601–610.

[45] Jentzen W, Freudenberg L, Eising E, Heinze M, Brandau W, Bockisch A, (2007), "Segmentation of PET volumes by iterative image thresholding," *J. Nucl. Med*, Vol. 48 (1), pp. 108–114.

[46] Judenhofer MS, et al, (2008), "Simultaneous PET-MRI: a new approach for functional and morphological imaging", *Nature Medicine*, Vol.14, pp.459–465.

[47] Ju W, Xiang D, Zhang B, Wang L, Kopriva I, Chen X, (2015), "Random Walk and Graph Cut for Co-Segmentation of Lung Tumor on PET-CT Images", *IEEE Transactions on Image Processing*, pp 1057-7149

[48] Kanakatte A, Gubbi J, Srinivasan B, Mani N, Kron T, Binns D, Palaniswami M, (2008), "Pulmonary tumor volume delineation in PET images using deformable models", *Proceeding of Engineering in Medicine and Biology Society, 30th Annual International Conference of the IEEE*, pp. 3118–3121.

[49] Koshy M, Paulino A, Howell R, Schuster D, Halkar R, Davis L, (2005), "F-18 FDG PET-CT fusion in radiotherapy treatment planning for head and neck cancer", *Head & neck*, Vol. 27, pp. 494–502.

[50] Kostakoglu L, Agress HJr, Goldsmith S, (2003), "Clinical role of FDG PET in evaluation of cancer patients", *Radiographics*, Vol.23(2), pp.315–340.

[51] Lardinois D, Weder W, Hany T, Kamel E, Korom S, Seifert B, von Schulthess G, Steinert H, (2003), "Staging of non-small-cell lung cancer with integrated positron-emission tomography and computed tomography", *New Engl J Med*, Vol.348(25), pp.2500–2507.

[52] Li H, Thorstad WL, Biehl KJ, Laforest R, Su Y, Shoghi KI, Donnelly ED, Low DA, Lu W, (2008), "A novel PET tumor delineation method based on adaptive region-growing and dual-front active contours", *Medical Physics*, Vol. 35, pp. 3711–3721.

[53] Lurig C, Kobbelt L, Ertl T, (2000), "Hierachical solutions for the deformable surface problem in visualization", *Graphical Models*, Vol 62, pp.2-18.

[54] MacManus MM, Nestle U, Rosenzweig K, Carrio I, Messa C, Belohlavek O, Danna M, Inoue T, Deniaud-Alexandre E, Schipani S, (2009), "Use of PET and PET/CT for radiation therapy planning: Iaea expert report 2006–2007", *Radiother Oncol*, Vol.1, pp.85–94.

[55] Markel D, Caldwell C, Alasti H, Soliman H, Ung Y, Lee J, Sun A, (2013), "Automatic segmentation of lung carcinoma using 3d texture features in 18-FDG PET/CT", *International Journal of Molecular Imaging*, Vol. 2013, ID. 980769 http://dx.doi.org/10.1155/2013/980769.

[56] Matheoud R, Della Monica P, Secco C, Loi G, Krengli M, Inglese E, Brambilla M, 2011, "Influence of different contributions of scatter and attenuation on the threshold values in contrast-based algorithms for volume segmentation", *Phys. Medica*, Vol. 27 (1), pp.44–51.

[57] Miller TR and Grigsby PW, (2002), "Measurement of tumor volume by PET to evaluate prognosis in patients with advanced cervical cancer treated by radiation therapy", *Int J Radiat Oncol Biol Phys*, Vol.53, pp.353–359.

[58] Montgomery D, Amira A, Zaidi H, (2007), "Fully automated segmentation of oncological PET volumes using a combined multiscale and statistical model", *Med Phys*, Vol.34(2), pp.722–736.

[59] Munley MT, Marks LB, Scarfone C, Sibley GS, Patz EF, Turkington TG, Jaszczak RJ, Gilland DR, Anscher MS, and Coleman RE, (1999), "Multimodality nuclear medicine imaging in three-dimensional radiation treatment planning for lung cancer: Challenges and prospects", *Lung Cancer*, Vol.23, No.2, pp.105–14.

[60] Murakami R et al, (2007), "Impact of FDG-PET/CT imaging on nodal staging for head-and-neck squamous cell carcinoma", *Int J Radiat Oncol Biol Phys*, Vol.68, pp.377–388.

[61] Nehmeh S, El-Zeftawy H, Greco C, Schwartz J, Erdi Y, Kirov A, Schmidtlein C, Gyau A, Larson S, Humm J, (2009), "An iterative technique to segment PET lesions using a monte carlo based mathematical model", *Med Phys*, Vol.36(10), pp.4803–4809.

[62] Nestle U, Kremp S, Grosu A, (2006), "Practical integration of 18f-FDG-PET and PET-CT in the planning of radiotherapy for non-small cell lung cancer (nsclc): the technical basis, icru-target volumes, problems, perspectives", *Radiother Oncol*, Vol.81(2), pp.209–225.

[63] Nestle U, Kremp S, Schaefer-Schuler A, Sebastian-Welsch C, Hellwig D, Rübe C, Kirsch C, (2005), "Comparison of different methods for delineation of 18f-FDG PET–positive tissue for target volume definition in radiotherapy of patients with non–small cell lung cancer", *J Nucl Med*, Vol.46, pp.1342–1348.

[64] Osher S and Fedkiw RP, 2003, *Level Set Methods and Dynamic Implicit Surfaces*, Springer, New York

[65] Otsu N, (1975), *A Threshold Selection Method from Gray-Level Histograms*, Automatica, pp:23-27.

[66] Otsu N, (1979), "A threshold selection method from gray-level histogram," *IEEE Trans-actions on Systems, Man, and Cybernetics*, Vol. 9, pp: 62–66.

[67] Paulino AC, Koshy M, Howell R, Schuster D, Daivs LW, (2005), "Comparison of CT- and FDG-PET-defined gross tumor volume in intensity-modulated radiotherapy for head-and-neck cancer", *International Journal of Radiation Oncology, Biology, Physics*, Vol.61, pp.1385–1392.

[68] Prieto E, Lecumberri P, Pagola M, Gómez M, Bilbao I, Ecay M, Peñuelas I, Martí-Climent J, (2012), "Twelve automated thresholding methods for segmentation of pet images: a phantom study", *Physics in Medicine and Biology*, Vol. 57, pp. 3963.

[69] Riegel A, Berson A, Destian S, et al, (2006), "Variability of gross tumor volume delineation in head-and-neck cancer using CT and PET/CT fusion", *International Journal of Radiation Oncology, Biology and Physics*, Vol.65(3), pp.726-732

[70] Rossi F and Abd Rahni AA, (2015), "Combination of low level processing and active contour techniques for semi-automated volumetric lung lesion segmentation from thoracic CT images", *Proceedings of IEEE Student Symposium in Biomedical Engineering & Sciences (ISSBES) Malaysia*, pp: 26-30, http://dx.doi.org/10.1109/ISSBES.2015.7435887

[71] Rossi F, Mokri SS, and Abd. Rahni AA, (2017), "Development of a semi-automated combined PET and CT lung Lesion segmentation framework", *Proceedings of SPIE - Progress in Biomedical Optics and Imaging*, Vol.10137B. http://dx.doi.org/10.1117/12.2256808

[72] Scarfone C, Lavely WC, Cmelak AJ, Delbeke D, Martin WH, Billheimer D, Hallaha DE, (2004), "Prospective feasibility trial of radiotherapy target definition for head and neck cancer using 3-dimensional PET and CT imaging", *Journal of Nuclear Medicine*, Vol.45(4), pp.543–552.

[73] Schaefer A, Kremp S, Hellwig D, Rübe C, Kirsch C, Nestle U, (2008), "A contrastoriented algorithm for FDG-PET-based delineation of tumour volumes for the radiotherapy of lung cancer: derivation from phantom measurements and validation in patient data", *Eur. J. Nucl. Med. Mol. Imaging*, Vol. 35 (11), pp.1989–1999

[74] Schinagl D, Vogel W, Hoffmann A, van Dalen J, Oyen W, Kaanders J, (2007), "Comparison of five segmentation tools for 18f-fluoro-deoxy-glucose–positron emission tomography–based target volume definition in head and neck cancer", *International Journal of Radiation Oncology, Biology and Physics*, Vol. 69, pp.1282–1289.

[75] Seute T, Leffers P, ten Velde G, Twijnstra A, "Detection of brain metastases from small cell lung cancer", *Cancer*, (2008), Vol.112 (8), pp.1827–1834.

[76] Sethian JA, (1999), *Level set methods and fast marching methods: evolving interfaces in computational geometry, fluid mechanics, computer vision, and materials science*, Vol. 3, Cambridge University Press, Cambridge, United, Kingdom

[77] Shah J, (1996), "Curve evolution and segmentation functionals: Application to color images", *Proceeding of the International Image Processing Conference, Lausanne, Switzerland, IEEE Int'l Conf. Image Proc.*, Vol. 9, pp. 461–464.

[78] Shankar LK, Hoffman JM, Bacharach S, Graham MM, et al, (2006), "Consensus recommendations for the use of 18F-FDG PET as an indicator of therapeutic response in patients in National Cancer Institute Trials", *J Nucl Med*, Vol.47, pp.1059–1066.

[79] Sharif MS, Abbod M, Amira A, Zaidi H, (2010), "Artificial neural network-based system for PET volume segmentation", *Int. Journal of Biomedical Imaging*, Vol. 2010, ID. 105610

[80] Song Q, Bai J, Han D, Bhatia S, Sun W, Rockey W, Bayouth J, Buatti J, Wu X, (2013), "Optimal co-segmentation of tumor in PET-CT images with context information", *IEEE Trans Med Imaging 32* , pp.1685–1697.

[81] Steenbakkers R, Duppen J, Fitton I, Deurloo K, Zijp L, Comans E, Uitterhoeve A, Rodrigus P, Kramer G, Bussink J, et al, (2006), "Reduction of observer variation using matched CT-PET for lung cancer delineation: a three-dimensional analysis", *Int J Radiat Oncol Biol Phys*, Vol.64(2), pp.435–448.

[82] Suri JS, Kecheng L, Singh S, Laxminarayan SN, Xiaolan Z, and Reden L, (2002), "Shape recovery algorithms using level sets in 2-D/3-D medical imagery: A state-of-the-art review," *IEEE Trans. Inf. Technol. Biomed.*, Vol. 6, pp. 8–28.

[83] van Dalen J, Hoffmann A, Dicken V, Vogel W, Wiering B, Ruers T, Karssemeijer N, Oyen W, (2007), "A novel iterative method for lesion delineation and volumetric quantification with FDG PET", *Nucl Med Commun*, Vol.28(6), pp. 293–485.

[84] Vees H, Senthamizhchelvan S, Miralbell R, Weber D, Ratib O, Zaidi H, (2009), "Assessment of various strategies for 18 f-FET PET-guided delineation of target volumes in high-grade glioma patients", *Eur. J. Nucl. Med. Mol. Imaging*, Vol. 36 (2), pp. 182–193.

[85] Wang X, Ballangan C, Cui H, et al, (2014), "Lung Tumor Delineation Based on Novel Tumor-Background Likelihood Models in PET-CT Images", *IEEE Transactions on Nuclear Science*, Vol. 61(1)

[86] Xiaa Y, Eberl S, Wena L, Fulhama M, Feng DD, (2012), "Dual-modality brain PET-CT image segmentation based on adaptive use of functional and anatomical information," *Computerized Medical Imaging and Graphics*, Vol. 36, pp. 47–53.

[87] Xu C, Pham DL, and Prince JL, (2002), *Handbook of Medical Imaging: Medical Image Processing and Analysis*, edited by Sonka M and Fitzpatrick JM, SPIE, Bellingham, WA, Vol.2, pp:129–174.

[88] Yang F, Grigsby P, (2012), "Delineation of FDG-PET tumors from heterogeneous background using spectral clustering", *Eur. J. Radiol.*, Vol. 81(11), pp. 3535–3541.

[89] Yu H, Caldwell C, Mah K, Mozeg D, (2009), "Coregistered FDG PET/CT-based textural characterization of head and neck cancer for radiation treatment planning", *IEEE Trans. Med. Imaging*, Vol. 28 (3), pp. 374–383.

[90] Zaidi H, Diaz-Gomez M, Boudraa A, Slosman D, (2002), "Fuzzy clustering-based segmented attenuation correction in whole-body pet imaging", *Physics in medicine and biology*, Vol. 47, pp.1143

[91] Zaidi H and El Naqa I, (2010), "Pet-guided delineation of radiation therapy treatment volumes: a survey of image segmentation technique", *European journal of nuclear medicine and molecular imaging*, Vol.37, pp.2165–2187.